Hindawi
Journal of Sensors
Volume 2022, Article ID 2020069, 11 pages
https://doi.org/10.1155/2022/2020069

*Research Article*

# Earthquake-Induced Ground Deformation Assessment via Sentinel-1 Radar Aided at Darbandikhan Town

**Farman Galeb Saed,[1] Abbas Mohammed Noori,[1,2] Bahareh Kalantar,[3] Waleed Mohammed Qader,[4] and Naonori Ueda[3]**

[1]*Department of Surveying Engineering, Technical Engineering College of Kirkuk, Northern Technical University, Kirkuk 36001, Iraq*
[2]*Geomatics Engineering Division, Civil Engineering Department, University of Technology, Baghdad, Iraq*
[3]*RIKEN Center for Advanced Intelligence Project, Goal-Oriented Technology Research Group, Disaster Resilience Science Team, Tokyo 103-0027, Japan*
[4]*Department of Civil Engineering, Cihan University-Erbil, Kurdistan Region, Iraq*

Correspondence should be addressed to Bahareh Kalantar; bahareh.kalantar@riken.jp

Received 27 October 2021; Revised 24 January 2022; Accepted 16 May 2022; Published 7 June 2022

Academic Editor: Antonio Lazaro



Deformation monitoring has conventional increasing consideration in recent years due to its great importance in modern engineering. Darbandikhan town was hit by a strong earthquake on 12th November 2017 which is the Sarpol-e Zahab earthquake. Interferometric Synthetic Aperture Radar (InSAR) technique has been used to investigate Darbandikhan town stability and the surrounding areas of the Kurdistan region in Iraq. The purpose of this research is to estimate the ground vertical displacement induced by the earthquake as well as the east-west deformation components. Moreover, previous research covered more of Iran's side country that the earthquake had an impact on with little on Iraq's side (Northern-eastern of Iraq), so it was worth researching on Darbandikhan town and surrounding structures to estimate the displacement on its infrastructures. For this study, two pairs of Sentinel-1 Synthetic Aperture Radar (SAR) images are used from each ascending and descending tracks over the study area to validate the work. Then, two differential interferograms are created from these images, along Darbandikhan town and the surrounding areas. These differential interferograms are then converted to line of sight (LOS) displacements using open source software (SNAP 8.0). The overall vertical displacement of the residential area of Darbandikhan was estimated from -4 to -10 cm after the earthquake, and the overall east-west displacement was ranging from 2 to 6.4 cm. The current study does not only examine the northern east of Iraq but the whole area of Iran and Iraq in general that lies within the influence of the earthquake. This research could be useful to estimate the overall deformation of Darbandikhan town in particular and the whole area in general. Therefore, the authorities and civil engineers could think of more sustainable buildings and structures before they start to plan within the area of earthquake impact.

## 1. Introduction

On 12 November 2017 at 21 : 18 local time, a very large earthquake, i.e., Sarpol-e Zahab, with a moment magnitude of 7.3 Mw struck the centre of Sarpol-e Zahab town which belongs to Kermanshah Province in Iran. The extreme earthquake has caused massive destruction of nearly most buildings in the Kermanshah province of Iran, killing more than 400 people and injuring more than 7,000. On the other side, this earthquake stretched to hit the Kurdistan region of Iraq, including Darbandikhan and Halabja (Figures 1(a) and 1(b)).

The most affected town was Sarpol-e Zahab, which had around 85, 000 inhabitants and collapsed on the sides of several tall buildings, resulting in multiple residents spending

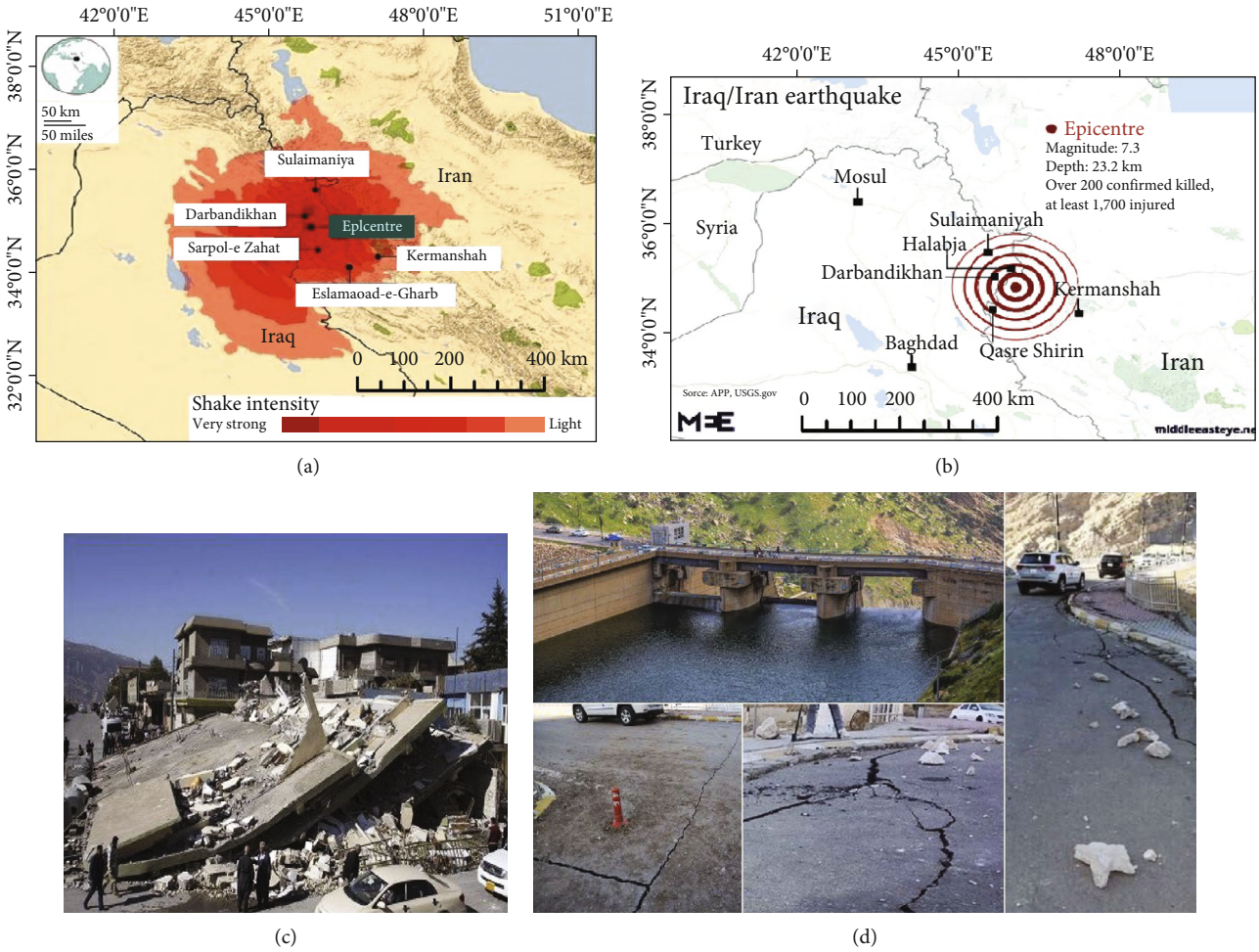


Figure 1: (a) The Sarpol-e Zahab showing the shake intensity (from right very strong shake to left lesser shake) earthquake adopted by (USGS 2017), (b) the earthquake impact on Kurdistan region and Iran (showing the area affected in thick red circles to light red circles) adopted by (reliefweb 2017), (c) Darbandikhan town with severe damage to their buildings, and (d) damages to the asphalt roads of Darbandikhan dam.

the night under freezing conditions. Most causalities who died and injured were in Iran's western Kermanshah province.

According to the Kurdish Regional Government (KRG), the earthquake (Sarpol-e Zahab) with a magnitude of 7.3 has left nine people dead and more than 500 people injured in Iraq especially in Darbandikhan and Halabja towns [1, 2]. The most severely affected area was Darbandikhan town with severe damage to their buildings such as collapse according to the World Health Organization (WHO) as shown in (Figures 1(c) and 1(d)). Based on the KRG, the earthquake also affected the infrastructure such as Darbandikhan's Tunnel and Darbandikhan's dam. A heavy amount of rocks fell down from the surrounding mountains onto the Darbandikhan tunnel causing the closure of the tunnel. The water and power network of the town were among the other most affected infrastructures by the earthquake. The multifunction embankment dam on the Diyala River in Darbandikhan was also badly affected by the earthquake and falling down rocks that have partially blocked the dam's spillway.

Remote sensing technology offers a large number of earth observation satellites that allow earth surface dynamic monitoring [3–5]. More recently, some remote sensing techniques were introduced to cover the deformation applications as an extra tool which can be added to the geodetic technique instrument for comparison and accuracy [6]. Deformation monitoring involves gathering information through field investigations along with remote sensing data, particularly radar interferometry techniques [7]. SAR is currently one of the most effective remote sensing data. Furthermore, the processing of the image by SAR sensors provides a special ability to identify high-resolution deformations and displacements in wide ranges region [8, 9].

*1.1. Literature Review.* Recently, radar interferometry was used for different applications, including digital elevation model production (DEM) [10], landslide monitoring [11–13], and deformation monitoring [14, 15]. There are many related works of deformation. For example, Crosetto et al. [16] used ERS and ENVISAT datasets in the Barcelona region to obtain a specific deformation estimate. Tofani et al.

[17] have combined ERS and ENVISAT sensors for the evaluation of a landslide problem with both ascending and descending geometries. García et al. [9] combined Sentinal-1 in descending geometry in the evaluation of the deformation of the City of Madrid. Gunce and San [18] used Sentinal-1 descending orbit to measure deformation in the south of Halabjah caused by the earthquake. Feng et al. [19] have combined Sentinal-1 and ALOS2 data with ascending and descending orbits for the assessment of coseismic deformation.

Differential InSAR (DInSAR) is an advanced technique of SAR interferometry that can detect surface displacement to a very high degree of accuracy. It is a change detection technique that was aimed at quantifying the relative movements in the scene between two SAR observations [20, 21]. The DInSAR technique uses the information contained in the phase of two SAR images to measure the shift between two corresponding pixels [22].

Sentinel-1 is the first of the Copernicus program satellite constellation conducted by the European Space Agency (ESA). The Copernicus program aims to provide information that will help to develop the climate change response, environmental management, and civil security within Europe [23]. Sentinel-1 is a collection of two identical, near-polar orbiting satellites. The first satellite, Sentinel-1A, was launched on 3rd April 2014, and the second, Sentinel-1B, was launched two years later. Both have demonstrated their efficacy in researching volcanic and seismic events as a timely response [24–28]. The capacity of the new sensor C-B and Sentinel-1 to collect SAR data worldwide in a quick overview will allow for the worldwide and regular tracking of ground surface deformations and present new challenges through cloud-based models [29]. The Interferometric Wide (IW) mode characteristically obtains SAR data of a greater spatial resolution which is $5 \times 20$ meters than Envisat/ASAR data (approximately 30 m). On the other hand, in comparison with 100 km Envisat/ASAR, SAR data occupies a 250 km range. These fundamental properties of the Sentinel-1 mission underline its significance, particularly in the sector of multitemporal InSAR analysis of deformation monitoring [30].

On the other hand, a single interferometric derived from a couple of SAR images is the base of classical DInSAR structure. In most cases, only one DInSAR configuration can be applied as the data availability is finite. Therefore, the key point to obtaining the best DInSAR regarding deformation monitoring is the total of available observations (interferograms). It is not potential to test the existed different errors that have an impact on interferometric observations.

There are many paper researches that use DInSAR regarding the coseismic deformations of the Sarpol-e Zahab earthquake. The researchers [31–34] used the same method of radar interferometry technique, namely, DInSAR, as it is a very powerful technique to observe the sudden change in the earth's topography during an earthquake. The approach is based on SAR interferometry, in which two images of an area before and after the incident are created at different times [20]. The phases of the matching pixels of two corresponding images are then compared and differenced, and altitude formation is derived from some basic arithmetic and image rectification. The phase of the microwave signal is changed and recorded on the platform, if there would be any physical change in the scene between two images. These phase changes convert to wrapped phase fringes; then, these wrapped fringes eventually convert into unwrapped phases to calculate the slant range deformation rate. Only one-dimensional changes (slant range) along the line of sight are measured with the SAR approach. However, this paper discusses the outcomes of the vertical displacement derived from slant range along the radar antenna as well as the horizontal component using some particular equations [35].

Having reviewed all literature reviews of the same research made on the Sarpol-e Zahab earthquake that occurred on 12th November 2017, none of the previous research papers focused on Darbandikhan town. In fact, Darbandikhan town was one of the most affected areas by the earthquake in the north of Iraq as it has different variety of infrastructures, including a big dam and a tunnel. Therefore, this paper particularly was aimed at presenting the vertical and east-west deformation map of the town using the differential interferometric SAR technique. In addition to that, a map of the whole region within the earthquake range was created using the coseismic and the postseismic SAR images, since the Sentinel-1 SAR images have a moderate geometric resolution (5 m by 20 m).

## 2. Study Area and Data Acquisition

*2.1. Study Area.* Darbandikhan town is located on an unstable shelf in a high folded zone [36]. The geological map of Sulaimaniya quadrangle and sheet NI-38-3 were obtained from the Ministry of Industry and Minerals (Iraq Geology Survey). Figure 2 shows the study area of Darbandikhan town in Sulaimaniya province in Iraq. Figure 3 shows that the town lies in three types of anticlines, Bamo anticline, Qaradagh anticline, and Balambo anticline [37, 38]. The Bamo anticline extends in the eastern part with 30 km length and 4 km width. The Qaradagh anticline lies in the southern part of the town by 10 km and 2.5 km in width. The Balambo anticline stretches in the northern part within an area of 50 km in length and roughly 2 km in width [39]. Furthermore, apart from the Sarpol-e Zahab earthquake in 2017, the area of Darbandikhan has not been subjected to any strong earthquake prior to this date.

*2.2. Data Acquisition.* Two sentinel SAR images in ascending orbit with another two pairs of SAR in descending orbit were used. The first image in ascending is dated back to 31 October 2017, and the second one is on 24 November, while the first and second images in descending orbit are dated back to 11 November 2017 and 17 November 2017, respectively (Table 1). The pixel resolutions of the Sentinel-1 IW1, IW2, and IW3 are $2.7 \times 22.5$, $3.1 \times 22.7$, and $3.5 \times 22.6$, respectively. The chain processes started from coregistration until the line of sight deformation (LOS) through SNAP6 software, and also, GIS 10.4 software was used to classify the deformation ranges.

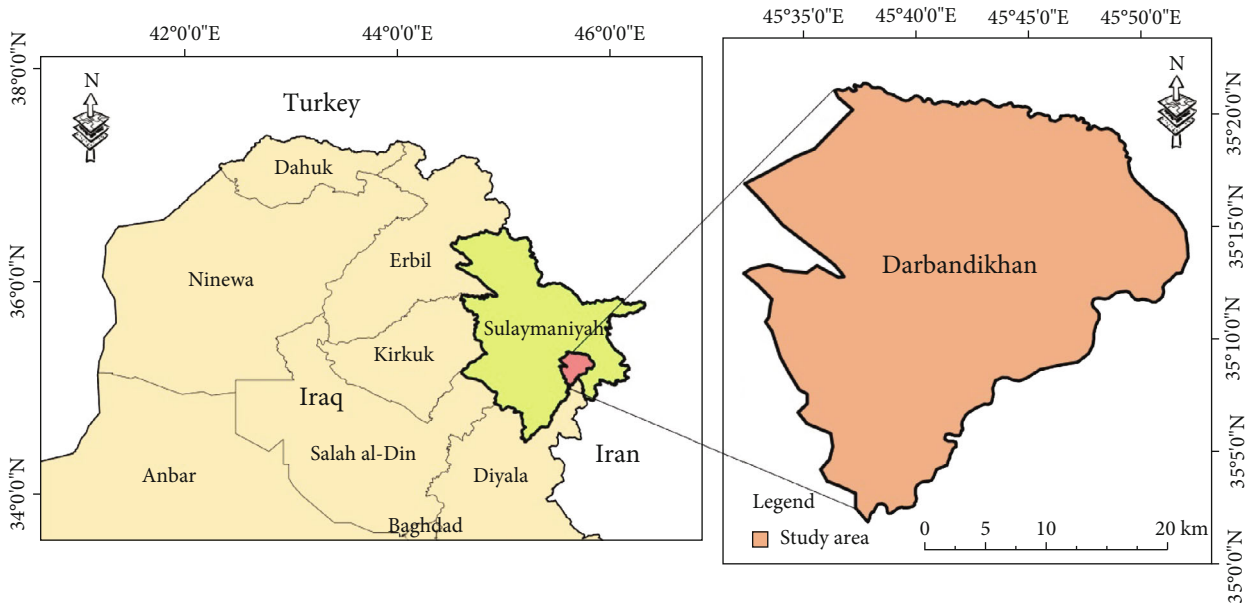


Figure 2: The study area (Darbandikhan City).

## 3. Methodology

*3.1. Differential Interferometric Synthetic Aperture Radar (InSAR).* Figure 4 shows the overall processing approach to find the differential interferograms over the region. DInSAR is a type of remote-sensing technique for measuring the deformation occurring between two satellite radar acquisitions. The satellite radar can detect deformation monitoring with respect to the earth's surface based on InSAR data. The satellite radar technique utilizes the data of two SAR images to obtain the differential map (Figure 5(a)). The InSAR phase is effectively able to detect digital terrain model (DTM) for lands and relative changes in elevation that occurs between two InSAR antennas crossing over the same lands, by differencing the corresponding phase content from the InSAR phase, leaving the content due to surface deformation of that area. Thus, the difference in elevations of terrain measurement can be determined. This method called differential InSAR technique, denote as DInSAR [22] which is the highest accurate mode of interferometric measurement. DInSAR data provides the common advantages of remote sensing techniques, which gives information over an unreachable large area of ground covers. In addition, it can effectively observe the high quality of deformation measurements. These are significant benefits with compare to geodetic technique measurements, such as total station and GPS, whereas, it is significant to say that the precision results can be obtained by using an adequate InSAR data with suitable statistical analysis of DInSAR data. SAR image technology can determine the elevations of objects on the ground through interferometry.

DInSAR is a type of remote-sensing technique for measuring deformation using two satellite radar acquisitions. The SAR satellite can detect ground motion with respect to Earth's surface based on InSAR. The DInSAR technique utilizes the data of two SAR images to obtain the differential map (Figures 5(a) and 5(b)).

The interferogram has several components, such as the topographic phase component and the noise component. The topographic phase component can be modeled and removed by using SRTM DEM, resulting in a differential interferogram, where it represents the surface changes between the two SAR acquisitions [22] which is the highest accurate mode of interferometric measurement. Also, it can effectively observe the high quality of deformation measurements. These are significant benefits compared to geodetic technique measurements, such as a total station and GPS.

There are some sources of error with respect to DInSAR observations: errors related to unwrapping, atmospheric, and residual topographic (due to DEM). The errors associated with unwrapping generally happen in weak coherence fields (areas), where the noise of the interferometric phase is high. The density of superb pixel may not be sufficient to get a precise deformation signal if the consistency is too low. The most negative errors could come from the large baseline and unknown DEM, which lie in residual errors. These sources of error limit the quality of the DInSAR technique that depends on a single interferogram. However, there are two other conditions that have to be considered: firstly, implementing an accurate DInSAR procedures such as registration of images, interferogram filtering, and phase unwrapping. Any changes in atmospheric refraction between two SAR observations could result in extra phase variations in a differential interferogram. There is much more delay in the phase of the SAR signal when penetrating through the thick atmosphere in the winter than in other seasons. Hence, to determine the pure deformation phase ($\Delta\varnothing def$), the components of the phase (atmospheric delay and the DEM errors, baseline errors, and random noise)

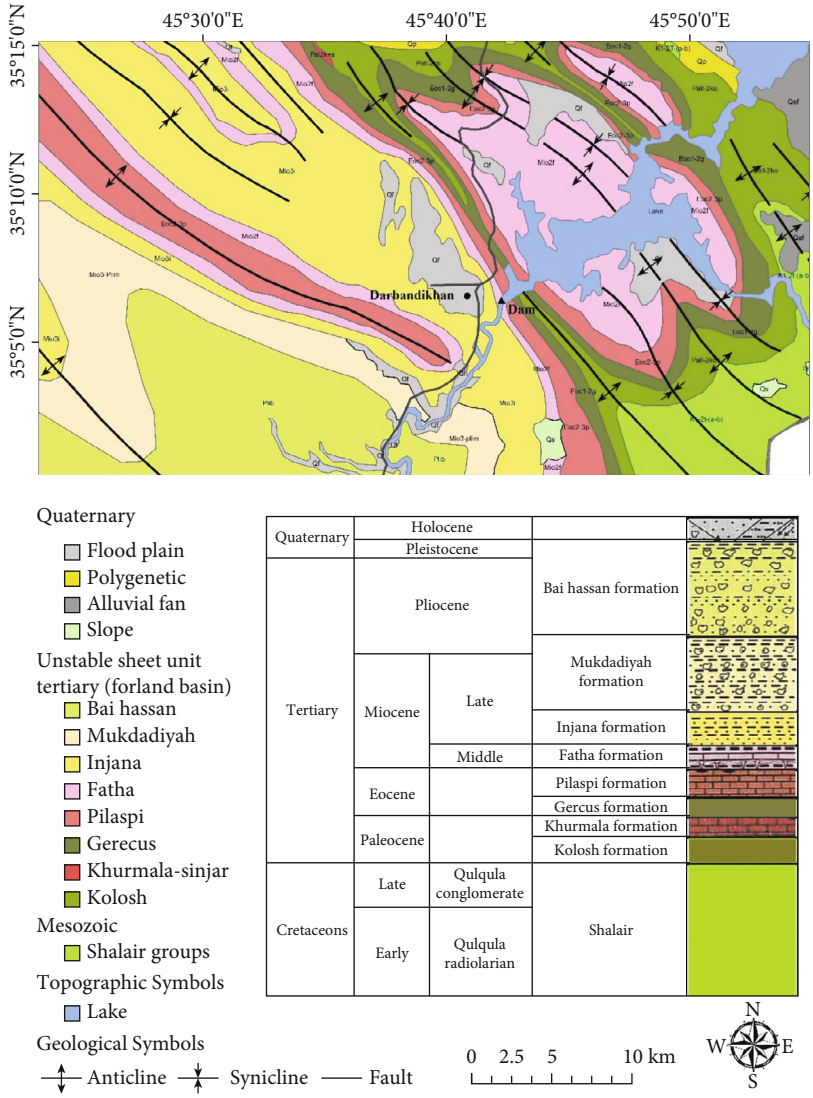


Figure 3: Geologic map and lithologic description of the study area.

Table 1: SAR data used.

| Mode | Date | Temp baseline | Perp baseline | Track | Orbit |
|---|---|---|---|---|---|
| Ascending | 11 Nov 2017-17 Nov 2017 | 6 days | 62 m | 72 | 192019-8323 |
| Descending | 31 Oct 2017-24 Nov 2017 | 24 days | 6 m | 79 | 19051-19401 |

need to be eliminated.

$$\Delta\Phi = \Delta\varnothing_{\text{defo}} + \Delta\varnothing_{\delta h} + \Delta\varnothing_{\text{APS}} + \Delta\varnothing_{B} + \Delta\varnothing_{n}, \quad (1)$$

where $\Delta\varnothing_{\text{defo}}$ = required deformation, $\Delta\varnothing_{\delta h}$ = DEM height errors, $\Delta\varnothing_{\text{APS}}$ = atmospheric delay, $\Delta\varnothing_{B}$ = orbital baseline errors, and $\Delta\varnothing n$ = random noise.

Finally, an accuracy assessment has been done for this study using descending data as test data. Descending orbit could use as an accuracy assessment technique to assess the outcomes gained by the ascending orbit [9, 17, 19].

*3.2. Preprocessing.* Image registration is a process for many applications such as remote sensing and photogrammetry as the images are acquired from different positions at different times. Coregistration was aimed at gaining an accurate overlap between two or more images relative to the same ground features. Hence, coregistration involves the alignment of a series of SAR interferometry images which need pixel-to-pixel matching between features in SAR image pairs from two antennas. Consequently, it is a necessary stage for the precise determination of phase difference and for noise reduction [40]. The parallax (disparity) between the SAR images is not visible as the approximate baseline between

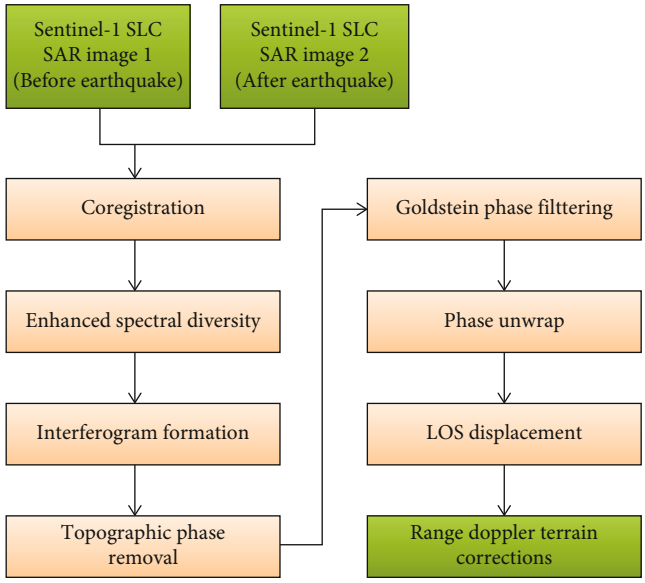


Figure 4: Overall methodology chart.

two images is 200 m with 850 km slant range distance. Hence, the whole aim of coregistration is to align the images for phase differencing. Another step needs to be performed before making the interferograms which is called resampling. It is usually the resampling of one complex SAR image a1 to project it onto a second image a2 within a precision of a tenth of a resolution element. Resampling can be viewed within two steps. Firstly, the continuous signal has to be reconstructed from its sampled version by looping (convolution) with interpolation kernel i (x; y). Secondly, make sampling for the reconstructed signal within new sampling grid.

### 3.3. Processing Approach

*3.3.1. Interferogram Generation and Phase Unwrapping.* The generation of the interferogram is formed by multiplying every single complex pixel of the master image with the corresponding conjugate complex pixel of the slave image.

$$P(X\,;Y) = S_1(x,y) * S_2(x,y), \tag{2}$$

$$P = S_1 * S_2, \tag{3}$$

where $P(x\,;y)$ is the interferogram pixel value of $(x\,;y)$,S1 is the pixel value of the master image at $(x\,;y)$, and $S * 2$ is the complex conjugate of the pixel value of the slave image at $(x\,;y)$.

The resulting differential interferogram is wrapped, where the pixel values are modulo $2\pi$. The phase differences across the interferogram will contain one or more $2\pi$ jumps. To determine the phase difference across the image, an integer number of $2\pi$ jumps must be detected and mathematically removed, and this is called phase unwrapping. In this case, the real unwrapped phase would be the mentioned value plus some integer multiple of 2?. The "sawtooth" fringes are transformed from individual straight lines to a smooth continuous curve.

Once the topographic contribution has been removed from the interferometric products [41], the result is a differential interferogram. When several points on the earth's surface are slowly changing their relative position (for example, in the event of subsidence, landslide, and earthquake) at different times between two SAR images, the additive phase term appears in the interferometric phase using the absolute interferometric phase as follows.

$$\Delta\varnothing = \frac{4\pi}{\lambda} d, \tag{4}$$

where $\Delta\varnothing$ is the phase difference between two SAR observations.

*3.3.2. Validation of the Results.* The combination of ascending and descending orbits of SAR images allows to compute the east-west displacement of the area of interest (Darbandikhan dam) [35] (Figure 5(b)). The differences of LOS projected deformation for all common pixels in the radar platform geometries for ascending and descending are computed. Moreover, the sum of LOS deformations for both different direction orbits ascending and descending is calculated. In short words, the vertical component of the ground displacement is related to the total amount of ascending/descending LOS-projected displacement. The difference between ascending and descending LOS, however, gives an estimation for the E-W component of the deformation. The following assumptions have been applied to the all LOS-projected deformation phase to obtain the vertical components along with east-west components of the displacement due to: firstly, ascending and descending LOS directions of the radar coincide in the east–z plane, and secondly, the radar sensor is approximately the same with ascending and descending orbits (Figure 5(b)). Equation (5) is used to determine the LOS to east-west displacement, and Equation (6) was used to find the LOS to vertical displacement.

$$d_{\text{Los}}^{(\text{East})} \approx \frac{d_{\text{Los}}^{(\text{Desc})} - d_{\text{Los}}^{(\text{Asc})}}{2\sin\varphi}, \tag{5}$$

$$d_{\text{Los}}^{(\text{Up})} \approx \frac{d_{\text{Los}}^{(\text{Desc})} - d_{\text{Los}}^{(\text{Asc})}}{2\cos\varphi}, \tag{6}$$

where

$d_{Los}^{(East)}$ is the line of sight displacement in the East-west direction

$d_{Los}^{(Up)}$ is the line of sight displacement in the vertical direction

$\cos\varphi$ and $\sin\varphi$ are the incident angles

## 4. Results

This section briefly discusses the results obtained over the Sarpol-e Zahab earthquake and its consequences on Darbandikhan town and Darbandikhan dam in terms of the vertical and east-west displacement. Two radar images in ascending

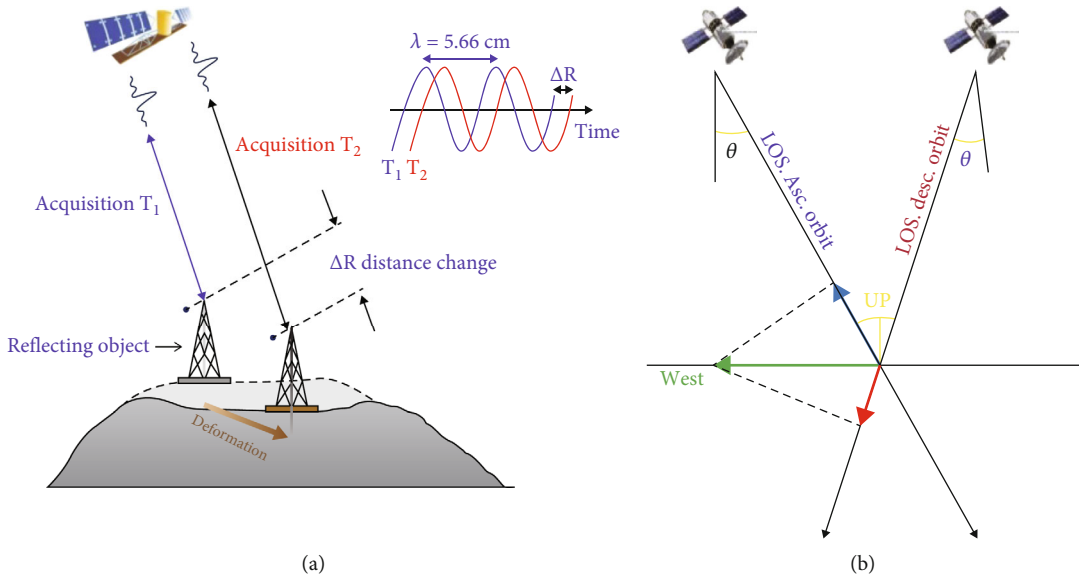


Figure 5: (a) Differential interferometry geometry between two acquisitions over the same target and (b) ascending and descending LOS.

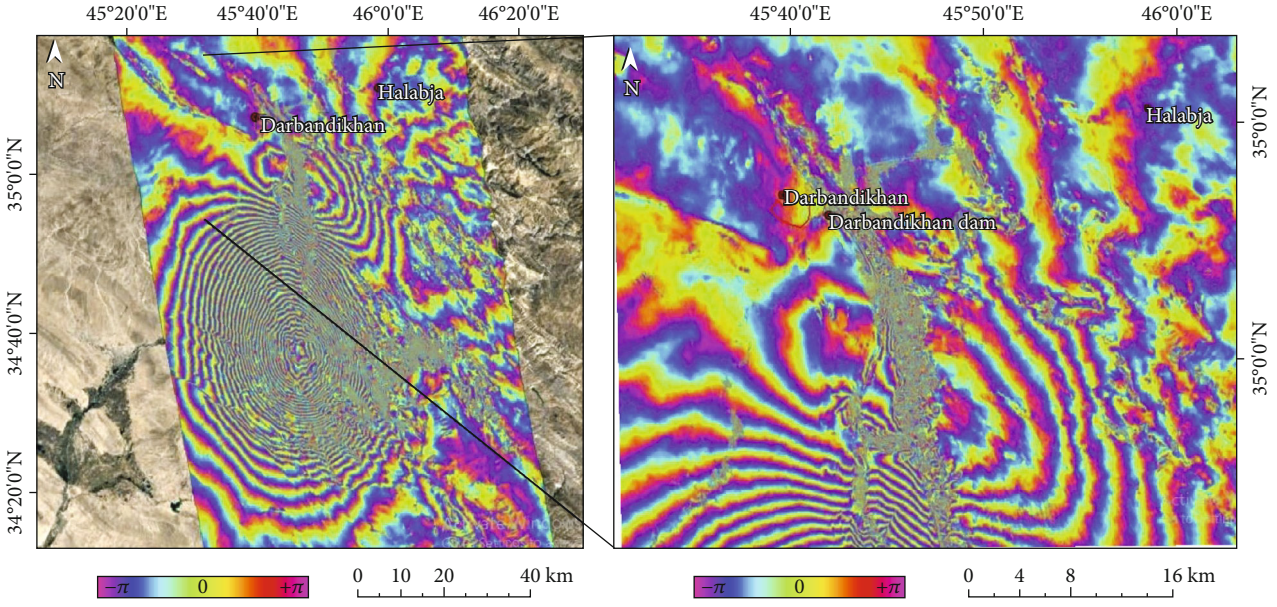


Figure 6: Differential interferograms over the region (Iran-Iraq border).

orbit coupled with another two images in descending orbit have been used in the processing. The time interval between the two images in ascending orbit and perpendicular bassline is 6 days with 62 m, respectively. Small perpendicular baselines are used to obtain highly coherent differential interferograms. The Sentinel1 has revealed thirty-one clear fringes over the region of the Iran and Iraq boundary due to the high magnitude of the earthquake with a few fringes over Darbandikhan town (Figure 6). This can be regarded as contours of deformation. In the high deformation regions, these colour limits are close to each other. As far as Darbandikhan town is concerned, the maximum vertical displacement has occurred over section AB, within the yellow polygon, with -7 to -10 cm subsidence (Figure 7) and the lowest subsidence was ranging from -4.1 to -7.1 cm in other parts of the town. In other words, the overall vertical displacement of the residential area of Darbandikhan was ranging from -4 to -10 cm after the earthquake on the 12$^{th}$ of November 2017. These displacement measurements revealed distance variations between the radar sensors and the ground. In regard to the Darbandikhan dam, a few points have been observed on the crest of the dam with approximately -10 cm down lift. The less-dense of observed points on the dam attributes to low coherence, and this was due to the position of the dam between two steep mountains which makes some of the backscatters hit the mountain

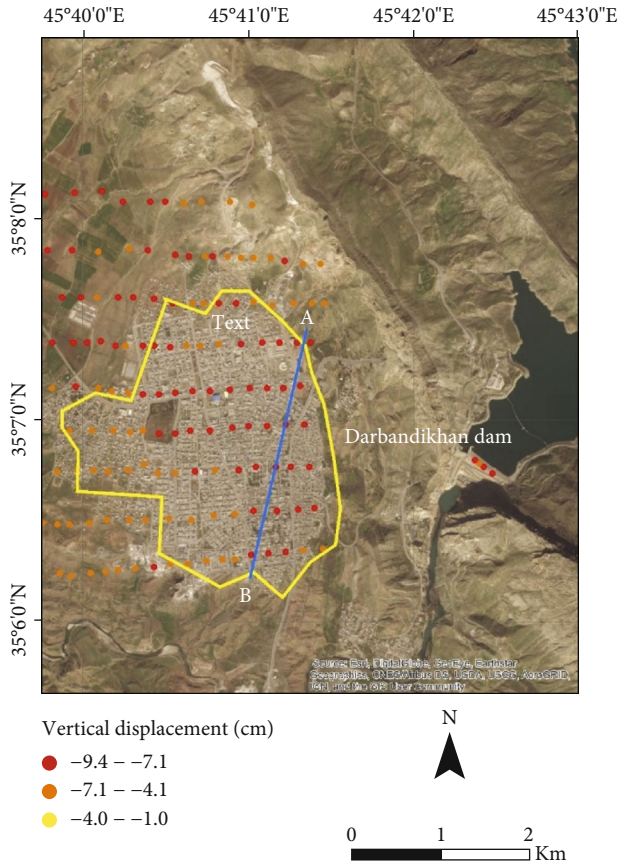


Figure 7: Vertical displacement map.

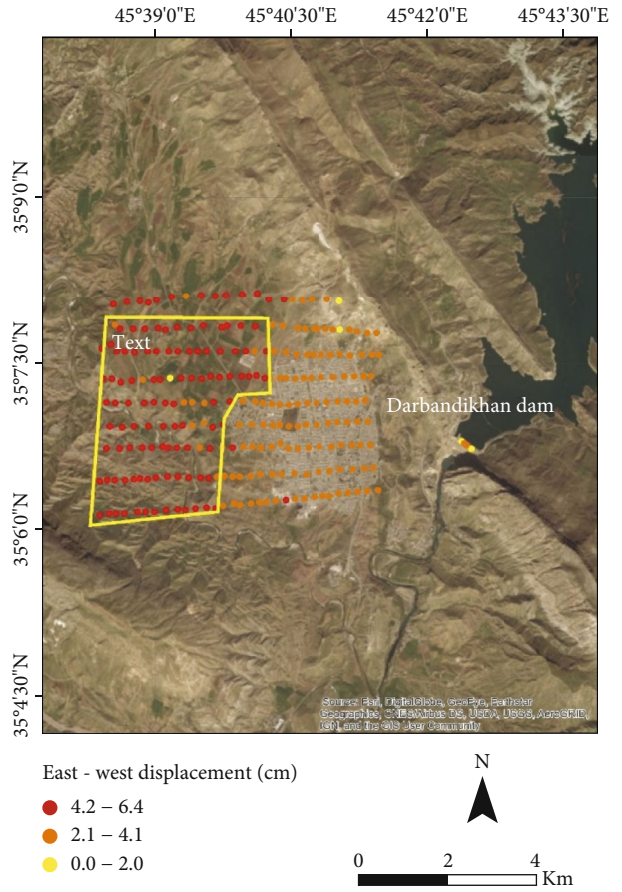


Figure 8: E-W displacement map.

and not get back to the radar sensor platform in the space. Furthermore, the low resolution of the Sentinel-1 images (5 m by 20 m) in comparison with the width of the dam made it difficult to observe too many points. In terms of east-west direction, the town has suffered a lesser motion with 2.1 to 4.1 cm in compare with -7 to -10 cm in a vertical motion Figures 7 and 8, while the east-west displacement of the observed points on the dam ranged between 2 and 4.1 cm.

There are a few radar interferometric techniques for monitoring deformation such as DInSAR, PSI, SBAS, and ISBAS. SAR technique covers a large area of ground which reaches 250 km swath at 5 m by 20 m spatial resolution. Moreover, it could effectively observe a high density of measurements over the area of interest. These are significant benefits compared to traditional monitoring methods including total station and GPS. The earlier papers [31] use the differential interferometric SAR (DInSAR) technique with different types of radar image data such as ALOS2 and Sentinel-1. And they use GAMMA software (commercial software) for SAR images processing, while this paper uses only noncommercial SAR images (Sentinel-1) along with Snap, free of charge software, which is available through the European Space Agency website. Most previous research papers, including [31, 32], studied the crest deformation regarding the basement fault of the North-West Zagros Fold-Thrust Belt zone deeply with complications of the geological formations of the area. However, this paper is concerned more with data processing with more details, subsidence (uplift and downlift), and horizontal movement over Darbandikhan town only during the 2017 Sarpol El-Zahab earthquake. And also, this research would give a deep insight into assessment in terms of distortion in all directions that took place in a very short moment of time.

## 5. Discussion

This study was conducted using free Sentinel-1 datasets from the ESA. Radar remote sensing is a very useful technique for deformation monitoring with compare to other traditional surveying methods, such as levelling, total station, and GNSS, and this is because the Sentinel-1 is an open source data (without any charge) and the coverage density is too high due to its large coverage 250 km × 150 km on the ground, while the GNSS technique grants one point or a few points depending on how many GNSS stations are available in the area of interest. It is worth mentioning that the deformation monitoring of earthquake does not need a series of images over time. This means the deformation of the earthquake can be covered with only two radar images (before and after the incident). To assess the results obtained from the ascending orbit, descending orbit was used as an accuracy assessment technique. Firstly, the ascending orbit has been used to find the displacement then the descending

Table 2: Accuracy assessment results.

| Point | Easting | Northing | Ascending vertical displacement (cm) | Descending vertical displacement (cm) |
|---|---|---|---|---|
| 1 | 45.68854 | 35.11948 | 4.0 | 4.2 |
| 2 | 45.68997 | 35.10942 | 4.0 | 4.1 |
| 3 | 45.67710 | 35.15566 | 4.7 | 5.6 |
| 4 | 45.66922 | 35.11242 | 3.3 | 4.3 |
| 5 | 45.62112 | 35.09967 | 3.8 | 4.3 |
| 6 | 45.67735 | 35.08043 | 3.4 | 4.4 |
| 7 | 45.68172 | 35.08605 | 3.3 | 4.1 |

orbit was used to assess the results. Table 2 shows the randomly selected points in the study area to assess the results. This assessment (descending) approved the ascending technique with almost similar results. Moreover, we observed a few points on the Darbandikhan dam structure, specifically in the middle, with up to -10 cm subsidence and 4 cm east-west displacement (Figure 7). The reason for the poor detection of the dam structure attributes to the low resolution of the Sentinel-1 images in compare with the width of the dam. So, a higher resolution radar imagery such as ICEYE is required for further investigation of the dam as it offers resolutions based on the size of the area captured, with a resolution reaches to 25 cm.

According to [31], the largest earthquake instrumentally recorded in the Iran-Iraq border region, the 2017 Mw7.3 Sarpol-e Zahab earthquake, is thought to have been caused by a basement fault at a depth of around 15 km in the north-west Zagros folded belt region. The results were based on the coseismic interferograms derived from ALOS-2 data. It observed that two slip asperities moved 6 m along 16 km in the best-fitting slip model. And also, during the earthquake, the Bamo Mount in the seismic zone was raised by around one meter. Based on [31] findings, the Zagros Fold-Thrust Belt zone is commonly known to be prone to both seismic and aseismic faulting. It is worth noting that the town of Darbandikhan is located approximately 65 kilometres from the epicentre of the Sarpol-e Zahab earthquake and has been affected as a result.

## 6. Conclusion

C-Band Sentinel-1 radar has shown its ability to detect the consequences of the Sarpol-e Zahab earthquake and also covered the whole scene of the incident due to its large coverage on the ground 250 km × 150 km (three subswaths) with a moderate resolution of 5 m by 20 m. This research has used two pairs of C-band Sentinel-1 images with two different orbits which are ascending and descending orbits. The combination of both SAR radar orbits served the research in two ways: firstly, the results obtained by a couple of descending orbits validated the same results (slightly different) from ascending one. Secondly, the combination allowed to compute the displacement in vertical and east-west directions. As mentioned, this study particularly was aimed at presenting the subsidence and east-west displacement map of the town using the differential interferometric technique. Moreover, a deformation map of the whole region within the earthquake range was created using the coseismic and the postseismic SAR images. The maximum vertical displacement occurred over section AB with -7 to -10 cm, and the lowest downlift displacement was ranging from -4.1 to -7.1 cm. The overall vertical displacement of the residential area of Darbandikhan was ranging from – 4 to -10 cm after the earthquake on 12$^{th}$ of November 2017. This piece of research could be used for future studies of the impacted area, Darbandikhan town, particularly in infrastructures including buildings, roads, and tunnels. More future work is needed for the purpose of monitoring the Drabandikhan dam using the latest, highest resolution SAR satellites such as TerraSAR-X (StripMap mode) which reaches up to 3 metre resolution.

## Data Availability

The data are available upon request.

## Conflicts of Interest

The authors declare that they have no conflicts of interest.

## Acknowledgments

For the new shared data from Sentinel-1, the authors wish to thank the European Satellite Agency (ESA) on the ESA website and also thank for their free SNAP.8 software. We would like to show our sincere appreciation to Prof. Dr. Qahtan Al-Nuaimy and Prof. Dr. Fawzi M. Omer at Northern Technical University for their perspective knowledge and help with the geologic map and lithology description in the study area.

## References

[1] "Reliefweb no title," 2017, https://reliefweb.int/report/iraq/earthquake-northeast-iraq-14-november-2017-1230-flash-update-3-enarku.

[2] USGS, *Generation of Earth's Surface Three-Dimensional (3-D) Displacement Time-Series by Multiple-Platform SAR Data. In Time Series Analysis and Applications*, IntechOpen, 2017, https://earthquake.usgs.gov/earthquakes/eventpage/us2000bmcg/executive#map.

[3] H. A. H. Al-Najjar, B. Kalantar, B. Pradhan et al., "Land cover classification from fused DSM and UAV images using convolutional neural networks," *Remote Sensing*, vol. 11, no. 12, 2019.

[4] B. Kalantar, N. Ueda, H. A. H. Al-Najjar, and A. A. Halin, "Assessment of convolutional neural network architectures for earthquake-induced building damage detection based on pre- and post-event orthophoto images," *Remote Sensing*, vol. 12, no. 21, p. 3529, 2020.

[5] S. Abdikan, F. B. Sanli, M. Ustuner, and F. Calò, "Land cover mapping using sentinel-1 SAR data," *International Archives of the Photogrammetry, Remote Sensing and Spatial Information Sciences*, vol. XLI-B7, pp. 757–761, 2016.

[6] F. Altıntaş and E. Gökalp, "Monitoring surface deformations of the reclamation site using PS interferometry: Senol Gunes sport complex (Turkey)," *Geocarto International*, vol. 1–13, pp. 1–14, 2021.

[7] P. Berardino, G. Fornaro, R. Lanari, and E. Sansosti, "A new algorithm for surface deformation monitoring based on small baseline differential SAR interferograms," *IEEE Transactions on Geoscience and Remote Sensing*, vol. 40, no. 11, pp. 2375–2383, 2002.

[8] K. Ahmadi, B. Kalantar, V. Saeidi, E. K. G. Harandi, S. Janizadeh, and N. Ueda, "Comparison of machine learning methods for mapping the stand characteristics of temperate forests using multi-spectral Sentinel-2 data," *Remote Sensing*, vol. 12, no. 18, p. 3019, 2020.

[9] A. J. García, M. Bakon, R. Martínez, and M. Marchamalo, "Evolution of urban monitoring with radar interferometry in Madrid City: performance of ERS-1/ERS-2, ENVISAT, COSMO-SkyMed, and Sentinel-1 products," *International Journal of Remote Sensing*, vol. 39, no. 9, pp. 2969–2990, 2018.

[10] H. A. Zebker and R. M. Goldstein, "Topographic mapping from interferometric synthetic aperture radar observations," *Journal of Geophysical Research - Solid Earth*, vol. 91, no. B5, pp. 4993–4999, 1986.

[11] G. Herrera, D. Notti, J. C. García-Davalillo et al., "Analysis with C-and X-band satellite SAR data of the Portalet landslide area," *Landslides*, vol. 8, no. 2, pp. 195–206, 2011.

[12] P. Lu, N. Casagli, F. Catani, and V. Tofani, "Persistent scatterers interferometry hotspot and cluster analysis (PSI-HCA) for detection of extremely slow-moving landslides," *International Journal of Remote Sensing*, vol. 33, no. 2, pp. 466–489, 2012.

[13] M. R. Mezaal and B. Pradhan, "An improved algorithm for identifying shallow and deep-seated landslides in dense tropical forest from airborne laser scanning data," *Catena*, vol. 167, pp. 147–159, 2018.

[14] P. Berardino, M. Costantini, G. Franceschetti, A. Iodice, L. Pietranera, and V. Rizzo, "Use of differential SAR interferometry in monitoring and modelling large slope instability at Maratea (Basilicata, Italy)," *Engineering Geology*, vol. 68, no. 1-2, pp. 31–51, 2003.

[15] G. E. Hilley, R. Bürgmann, A. Ferretti, F. Novali, and F. Rocca, "Dynamics of slow-moving landslides from permanent scatterer analysis," *Science*, vol. 304, no. 5679, pp. 1952–1955, 2004.

[16] M. Crosetto, E. Biescas, J. Duro, J. Closa, and A. Arnaud, "Generation of advanced ERS and Envisat interferometric SAR products using the stable point network technique," *Photogrammetric Engineering and Remote Sensing*, vol. 74, no. 4, pp. 443–450, 2008.

[17] V. Tofani, F. Raspini, F. Catani, and N. Casagli, "Persistent Scatterer Interferometry (PSI) technique for landslide characterization and monitoring," *Remote Sensing*, vol. 5, no. 3, pp. 1045–1065, 2013.

[18] H. B. Gunce and B. T. San, "Measuring earthquake-induced deformation in the south of Halabjah (Sarpol-e-Zahab) using Sentinel-1 data on November 12, 2017," *Multidisciplinary Digital Publishing Institute Proceedings*, vol. 2, p. 346, 2018.

[19] G. Feng, Z. Li, B. Xu, X. Shan, L. Zhang, and J. Zhu, "Coseismic deformation of the 2015$M_w$ 6.4 Pishan, China, earthquake estimated from Sentinel-1A and ALOS2 data," *Seismological Research Letters*, vol. 87, no. 4, pp. 800–806, 2016.

[20] A. K. Gabriel, R. M. Goldstein, and H. A. Zebker, "Mapping small elevation changes over large areas: differential radar interferometry," *Journal of Geophysical Research - Solid Earth*, vol. 94, no. B7, pp. 9183–9191, 1989.

[21] A. Sowter, L. Bateson, P. Strange, K. Ambrose, and M. F. Syafiudin, "DInSAR estimation of land motion using intermittent coherence with application to the south Derbyshire and Leicestershire coalfields," *Remote Sensing Letters*, vol. 4, no. 10, pp. 979–987, 2013.

[22] M. Crosetto, A. Arnaud, J. Duro, E. Biescas, and M. Agudo, "Deformation monitoring using remotely sensed radar interferometric data," in *Proceedings of the 11th FIG Symposium on Deformation Measurements*, Santorini, Greece, 2003.

[23] Z. Malenovský, H. Rott, J. Cihlar et al., "Sentinels for science: potential of Sentinel-1, -2, and -3 missions for scientific observations of ocean, cryosphere, and land," *Remote Sensing of Environment*, vol. 120, pp. 91–101, 2012.

[24] P. J. González, M. Bagnardi, A. J. Hooper et al., "The 2014–2015 eruption of Fogo volcano: geodetic modeling of Sentinel-1 TOPS interferometry," *Geophysical Research Letters*, vol. 42, no. 21, pp. 9239–9246, 2015.

[25] J. R. Elliott, R. Jolivet, P. J. González et al., "Himalayan megathrust geometry and relation to topography revealed by the Gorkha earthquake," *Nature Geoscience*, vol. 9, no. 2, pp. 174–180, 2016.

[26] R. Grandin, E. Klein, M. Métois, and C. Vigny, "Three-dimensional displacement field of the 2015 $M_w$8.3 Illapel earthquake (Chile) from across- and along-track Sentinel-1 TOPS interferometry," *Geophysical Research Letters*, vol. 43, no. 6, pp. 2552–2561, 2016.

[27] D. Melgar, W. Fan, S. Riquelme et al., "Slip segmentation and slow rupture to the trench during the 2015, $M_w$8. 3 Illapel, Chile earthquake," *Geophysical Research Letters*, vol. 43, no. 3, pp. 961–966, 2016.

[28] M. Polcari, M. Palano, J. Fernández, S. V. Samsonov, S. Stramondo, and S. Zerbini, "3D displacement field retrieved by integrating Sentinel-1 InSAR and GPS data: the 2014 South Napa earthquake," *European Journal of Remote Sensing*, vol. 49, no. 1, pp. 1–13, 2016.

[29] M. Costantini, F. Minati, M. G. Ciminelli, A. Ferretti, and S. Costabile, "Nationwide ground deformation monitoring by persistent scatterer interferometry," in *2015 IEEE International Geoscience and Remote Sensing Symposium (IGARSS)*, pp. 1472–1475, Milan, Italy, 2015.

[30] F. Costantini, A. Mouratidis, G. Schiavon, and F. Sarti, "Advanced InSAR techniques for deformation studies and for simulating the PS-assisted calibration procedure of Sentinel-1 data: case study from Thessaloniki (Greece), based on the Envisat/ASAR archive," *International Journal of Remote Sensing*, vol. 37, no. 4, pp. 729–744, 2016.

[31] W. Feng, S. Samsonov, R. Almeida et al., "Geodetic constraints of the 2017 $M_w$7.3 Sarpol Zahab, Iran earthquake, and its implications on the structure and mechanics of the Northwest Zagros Thrust- Fold Belt," *Geophysical Research Letters*, vol. 45, no. 14, pp. 6853–6861, 2018.

[32] Y. Yang, J. Hu, A. Yassaghi et al., "Midcrustal thrusting and vertical deformation partitioning constraint by 2017 $M_w$ 7.3 Sarpol Zahab earthquake in Zagros Mountain Belt, Iran," *Seismological Research Letters*, vol. 89, no. 6, pp. 2204–2213, 2018.

[33] S. Vajedian and M. Motagh, "Coseismic displacement analysis of the 12 November 2017 Mw 7.3 Sarpol-e Zahab (Iran) earthquake from SAR Interferometry, burst overlap interferometry

and offset tracking," *ISPRS Annals of the Photogrammetry, Remote Sensing and Spatial Information Sciences*, vol. 4, pp. 205–209, 2018.

[34] I. Ashayeri, M. A. Memari, and E. Haghshenas, "Seismic microzonation of Sarpol-e-zahab after Mw 7.3 2017 Iran earthquake: 1D-equivalent linear approach," *Bulletin of Earthquake Engineering*, vol. 19, pp. 605–622, 2021.

[35] A. Pepe and F. Calò, "A review of interferometric synthetic aperture RADAR (InSAR) multi-track approaches for the retrieval of Earth's surface displacements," *Applied Sciences*, vol. 7, no. 12, p. 1264, 2017.

[36] S. Z. Jassim and J. C. Goff, *Geology of Iraq*, DOLIN, Sro, Distributed by Geological Society of London, 2006.

[37] F. A. A. Lawa and A. A. Ghafur, "Sequence stratigraphy and biostratigraphy of the prolific late Eocene, Oligocene and early Miocene carbonates from Zagros fold-thrust belt in Kurdistan region," *Arabian Journal of Geosciences*, vol. 8, no. 10, pp. 8143–8174, 2015.

[38] Q. A. M. Al Nuaimy, "Morphometric analysis of Chattian–Early Aquitanian Miogypsinidae from Iraq and their stratigraphic distribution in the Arabian Tethys," *Arabian Journal of Geosciences*, vol. 10, no. 24, pp. 1–17, 2017.

[39] S. Sadeghi and A. Yassaghi, "Spatial evolution of Zagros collision zone in Kurdistan, NW Iran: constraints on Arabia–Eurasia oblique convergence," *Solid Earth*, vol. 7, no. 2, pp. 659–672, 2016.

[40] Z. Li and J. Bethel, "Image coregistration in SAR interferometry," *The International Archives of the Photogrammetry, Remote Sensing and Spatial Information Sciences*, vol. 37, pp. 433–438, 2008.

[41] M. Besoya, H. Govil, and P. Bhaumik, "A review on surface deformation evaluation using multitemporal SAR interferometry techniques," *Spatial Information Research*, vol. 29, no. 3, pp. 267–280, 2021.